

Article

# Petrogenetic Implications for Ophiolite Ultramafic Bodies from Lokris and Beotia (Central Greece) Based on Chemistry of Their Cr-spinels

Panagiotis Pomonis \* and Andreas Magganas

Department of Geology and Geoenvironment, National and Kapodistrian University of Athens, Panepistimioupolis Zografou, 15784 Athens, Greece; amagganas@geol.uoa.gr

\* Correspondence: ppomonis@geol.uoa.gr; Tel.: +30-210-727-4844

Academic Editors: Basilios Tsikouras, Antonio Acosta-Vigil and Jesus Martinez-Frias

Received: 29 December 2016; Accepted: 24 February 2017; Published: 3 March 2017

**Abstract:** Cr-spinels from ultramafic rocks from Lokris (Megaplatanos and Tragana), and Beotia (Ypato and Alyki) ophiolitic occurrences were studied. These rocks comprise principally harzburgite with minor dunite. Small amounts of clinopyroxene-rich harzburgite and lherzolite have been observed along with the harzburgite in Alyki. The Cr# in the studied spinels displays a wide variability. The spinels hosted in harzburgite and cpx-rich harzburgite display low Cr# (<0.6), typical for oceanic (including back-arc basins) ophiolites, whereas the spinels hosted in dunite with Cr# (>0.6) characterize arc-related ophiolitic sequences. Cr-spinels from Alyki indicate a moderate fertile character and are analogous to those from abyssal peridotites. The dunitic and harzburgitic spinel–olivine pairs are consistent with a Supra-Subduction Zone origin. The relatively large range in spinel Cr# and Mg# may have been resulted from a wide range of degrees of mantle melting during the evolution of the host peridotites.

**Keywords:** peridotite; harzburgite; lherzolite; dunite; chromite; mantle melting; abyssal; olivine

## 1. Introduction

Chromian spinel is a common mineral in peridotites of ophiolite complexes. It has a wide range in composition and serves as an important petrogenetic indicator for ultramafic and related rocks [1]. Since the chemical composition of spinels depends on several petrogenetic factors (e.g., crystallization from melt, residue after partial melting with variable degrees, crystallization via melt–peridotite interaction) and physical conditions (pressure, temperature, oxygen fugacity) of the host peridotites, e.g., [2–4], they can be correlated with different tectonic settings, e.g., [1,2,4–11]. Cr- and Al-rich chromites occur usually in the upper-mantle part of the ophiolite pseudosection or close to the crust–mantle boundary, and less commonly in the lowermost oceanic crust. In the last three decades, most authors have agreed that ophiolitic chromitites, consisting mainly of Cr- and Al-rich spinels, have formed during melt–rock reaction and/or melt–melt interaction in the mantle section of supra-subduction zone (SSZ) ophiolites, e.g., [1,12–23]. The Cr# [= Cr/(Cr + Al) atomic ratio] of chromian spinel is an important geochemical parameter for the estimation of the degree of partial melting and provenance of peridotites [24].

In this paper, we present for the first time petrographical and mineral chemical data of four dismembered ophiolite slices, Ypato, Alyki, Tragana and Megaplatanos, located in the Beotia and Lokris area of central Greece. These ophiolitic occurrences are mainly composed of mantle peridotites with disseminated chromian spinel and constitute part of the southern prolongation of the NW–SE trending ophiolite belt that includes the Albanian and Dinaric ophiolites further north in the Balkan Peninsula (Figure 1). They occupy a key position between the External and Internal Hellenides (Figure 1) as a

link between the Othris and Kallidromon Mountains to the north that host a well-preserved ophiolite sequence and the Argolis peninsula to the south, where ophiolitic rocks are not so voluminous and outcrop as dismembered bodies.

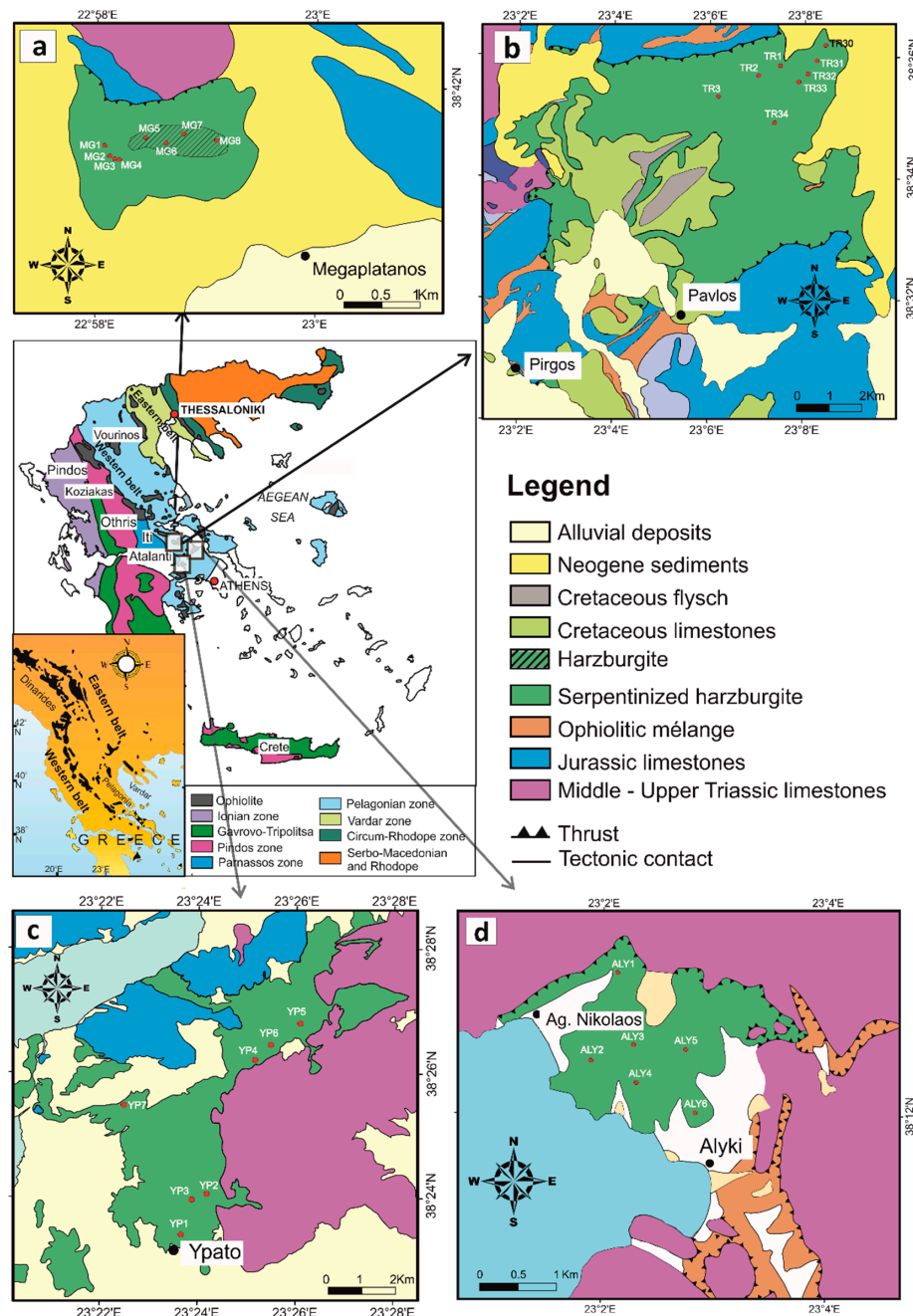


**Figure 1.** Geological maps with the sample locations of (a) Megaplatanos; (b) Tragana; (c) Ypato; and (d) Alyki ophiolites. Inset shows a simplified geological map of Greece with the main isopic zones and the distribution of ophiolite occurrences in Balkan Peninsula.

## 2. Geological Setting

The ophiolitic rocks in Greece are part of the Tethyan ophiolitic belt, which extends from central Europe throughout the eastern Mediterranean area and up to the Himalayas. The Beotia and Lokris ophiolitic occurrences are located in central Greece and belong to the western part of the Dinaric-Hellenic ophiolite belt (Figure 1). The studied ophiolitic bodies are dismembered and appear

in the form of imbricated thrust sheets that tectonically overlie Triassic–Jurassic formations of the west Pelagonian margin zone, which corresponds to the western side of the Pelagonian continental block [25,26]. Ophiolitic mélangé formations, which additionally comprise clastic components of varied size, are found tectonically emplaced above Palaeozoic to Jurassic formations. The west Pelagonian margin ophiolitic units are interpreted to be remnants of a relatively small Jurassic Neotethyan oceanic basin. It has long been debated whether these west Pelagonian margin ophiolites originated from the micro-oceans of Pindos or Vardar. In the former case, the Pindos micro-ocean was located between the elongated micro-continental Pelagonian block and Gondwana, while Vardar micro-ocean existed between the Pelagonian block and Laurasia. In the second case, the west Pelagonian margin ophiolites are Vardarian westwards far-travelled nappes, which during the Upper Jurassic–Lower Cretaceous period obducted the Pelagonian block, thus representing the easternmost continental promontory of Gondwana [27,28]. The Megaplatanos ophiolite (Figure 1a) is a small ultramafic body consisting of serpentinite, serpentinitised harzburgite and harzburgite veined by a dense stockwork of magnesite. Serpentinite is restricted to the western part of the studied area while the central and eastern part is dominated by serpentinitised harzburgite and harzburgite with veins of magnesite (Figure 2a). Locally, dunite with disseminated spinel grains forms thin layers that are a few cm to a few dm thick, intercalated in the harzburgite. The peridotites tectonically overlie to the north Middle–Upper Triassic and Jurassic limestones, while they are unconformably overlain by fluvio-terrestrial clastic sediments and Holocene age alluvial deposits.

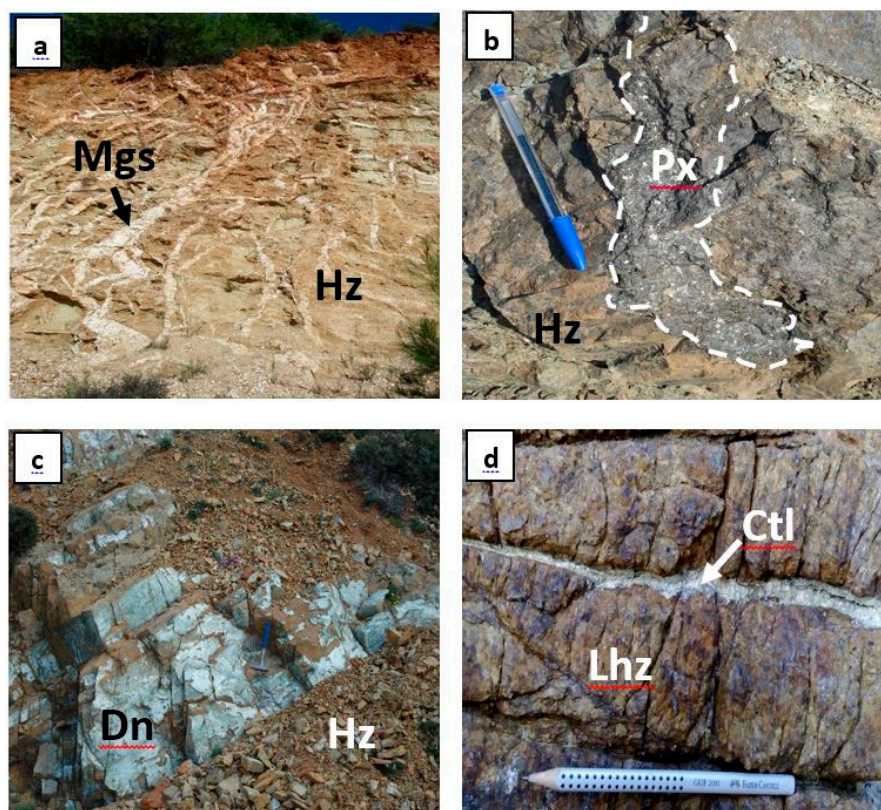


**Figure 2.** Photographs of the studied ophiolite occurrences: (a) Stockwork of magnesite in massive harzburgite (Megaplatanos); the horizontal scale is ~4 m; (b) Pyroxenite dyke intruding into serpentinitised harzburgite (Alyki); (c) Dunite layers intercalated with cataclastic harzburgite (Ypato); (d) Cross-fibre chrysotile dyke crosscutting coarse-grained lherzolite (Alyki). Abbreviations: Mgs–Magnesite, Hz–Harzburgite, Px–Pyroxenite, Dn–Dunite, Lhz–Lherzolite, Ctl–Chrysotile.

The Tragana ophiolite nappe comprises mainly serpentinite and serpentinitised harzburgite with minor dunite (Figure 1b). Rare chromitite horizons, of up to 2 cm in thickness, are present

in dunitic layers. Well-developed foliation and associated lineation of mineralogical constituents of serpentinitised harzburgite suggest intense high-temperature plastic deformation in the peridotites. The Tragana peridotites tectonically overlie the ophiolitic mélangé that is characterized by a chaotic and heterogeneous mixture composed of rock fragments of spilites, altered gabbro, red chert and serpentinitised peridotite incorporated in a tectonised multi-coloured argillaceous matrix. The Tragana ophiolite nappe is unconformably overlain by Upper-Cretaceous transgressive formations and Neogene sedimentary rocks.

The Ypato ophiolite (Figure 1c) represents a remnant ultramafic nappe comprising serpentinitised harzburgite, harzburgite and serpentinite veined by a sparse network of pyroxenite dykes (Figure 2b). Fresh harzburgite outcrops are restricted to the central part of the ophiolite body, with intercalations of thin dunite layers (Figure 2c). The ultramafic nappe is in tectonic contact with Middle-Upper Triassic and Jurassic limestones. Tectonic deformation resulted in fracturing, faulting and shearing throughout the ultramafic nappe.

The Alyki ophiolite body (Figure 1d) is mainly made up of serpentinitised harzburgite clinopyroxene-rich harzburgite and lherzolite. The main part of the ultramafic rocks is composed of typical harzburgite with <4% of modal clinopyroxene, along with m-scale to 50 m-scale domains of clinopyroxene-rich harzburgite (cpx-rich hereinafter) and sparse lherzolite with ~5%–10% modal clinopyroxene (Figure 2d). The local gradations of typical to cpx-rich harzburgite and lherzolite show no systematic structural pattern and are most commonly observed in the central and south parts of the study area between the small ports of Agios Nikolaos and Alyki. Dunite is occasionally found as lenses, a few cm to dm thick, throughout the harzburgite mass. A sparse network of pyroxenite veins of some millimetres to some centimetres in size cross-cut the mantle rocks. The peridotites are in tectonic contact with an ophiolitic, tectonic mélangé consisting of fragments of gabbro, dolerite, basalt, red chert, sandstone, limestone and serpentinitised peridotite surrounded by a tectonised, multi-coloured, clayey matrix. The ophiolitic nappe of Alyki is overthrust onto Middle-Upper Triassic limestones, while it is unconformably overlain by alluvial deposits.

### 3. Materials and Methods

Rock samples were collected from the ophiolitic occurrences of Megaplatanos, Tragana, Ypato and Alyki during detailed fieldwork. Care was taken to sample the least altered and most representative rocks from different lithologies. Fifty-two thin and polished-thin sections were examined using a polarizing, transmitted light microscope equipped with a digital camera. Microanalyses and scanning electron microscope (SEM) observations were carried out at the University of Athens, Department of Geology and Geoenvironment, using a JEOL JSM 5600 SEM, equipped with automated energy dispersive analysis system ISIS 300 OXFORD, with the following operating conditions: accelerating voltage 20 kV, beam current 0.5 nA, time of measurement 50 s and beam diameter 1–2  $\mu\text{m}$ . The spectra were processed using a ZAF program (three iterations). Synthetic oxides and natural minerals were utilized as standards for our analyses. Detection limits are ~0.1% and an accuracy better than 5% was obtained. Selected crystals of spinel-group minerals in polished thin sections of harzburgite, dunite and lherzolite were analysed across profile lines in order to assess compositional variation.

### 4. Results

#### 4.1. Petrography

The ultramafic samples collected from the study areas comprise variably serpentinitised harzburgite and lesser dunite and clinopyroxene-rich harzburgite that grade to lherzolite. The degree of serpentinitization ranges between 10% and 80% and increases from dunite to harzburgite and lherzolite. The two commonest textures observed are medium to coarse-grained porphyroclastic and granular. Variable amounts of serpentine, chlorite, tremolite and magnetite are observed in the studied rocks as products of alteration.

The harzburgite samples show porphyroclastic to mylonitic textures (Figure 3a). Their primary modal mineralogy includes olivine (65–80 vol. %), orthopyroxene (15–30 vol. %) and spinel (up to 5%). The first two minerals usually display undulose extinction, strain lamellae, kink bands, rotation, shearing, due to plastic deformation, as well as recrystallization (Figure 3a). These structures are typical features of Alpine-type upper mantle peridotites. Olivine forms porphyroclastic grains (<2 mm), as well as smaller polygonal neoblasts (~0.2 mm) with 120° triple junctions. The orthopyroxene forms isolated large crystals with lobate boundaries and often displays diopside exsolution lamellae, kink bands and gliding parallel to (001). Dark-brown coloured chromium-rich spinels (Figure 3b) commonly form subhedral to anhedral grains (<3mm) with lobate boundaries, usually veined and surrounded by a rim of magnetite developed during alteration (Figure 3c). In some cases, spinels contain small olivine inclusions.

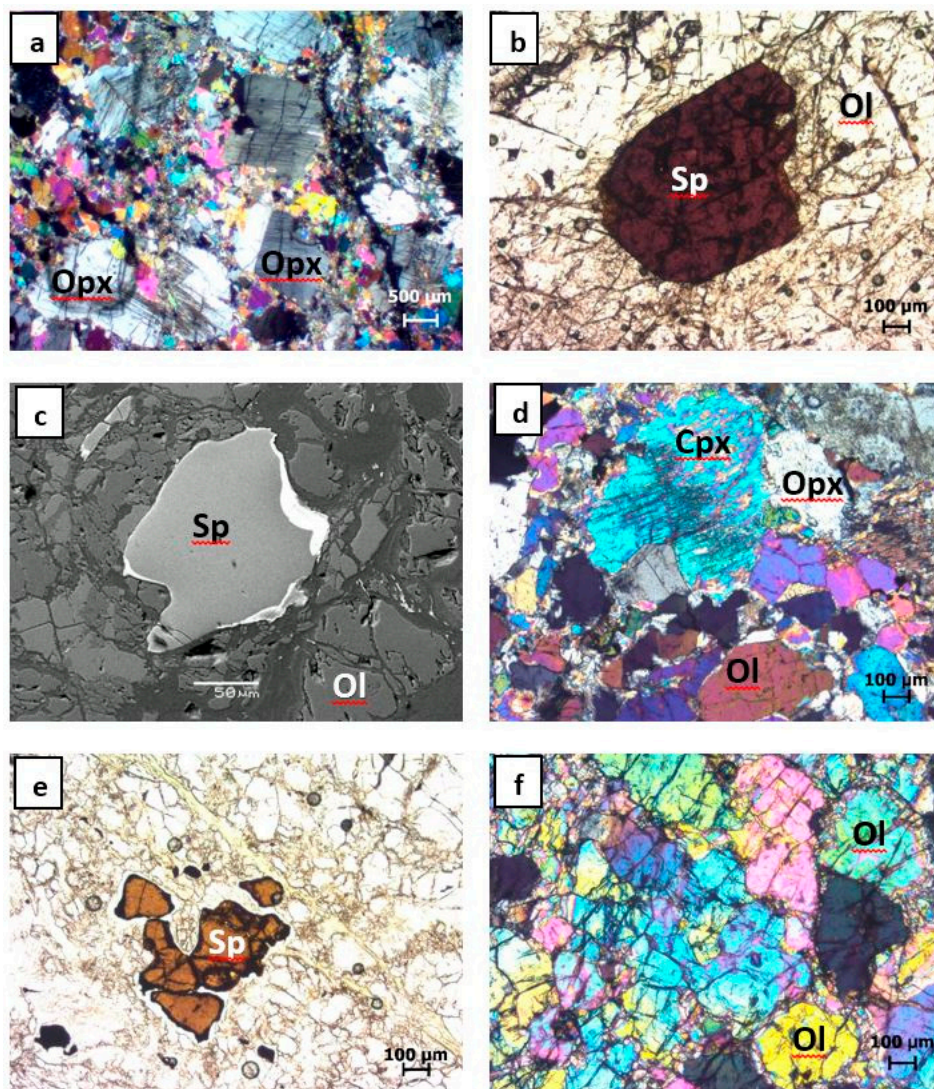


**Figure 3.** Photomicrographs of the studied mantle peridotites: (a) Porphyroclastic texture in harzburgite. Orthopyroxene porphyroclasts show undulose extinction, strain lamellae, kink bands, rotation, shearing and recrystallization (XPL, sample MG1, Megaplatanos); (b) Dark-brown coloured hypidiomorphic spinel grain in harzburgite (PPL, sample TR5, Tragana); (c) Back-scattered electron image of a spinel surrounded by magnetite (sample YP3, Ypato); (d) Porphyroclastic texture in lherzolite (XPL, sample ALY2, Alyki); (e) Light-brown coloured Al-spinel with lobate boundaries (PPL, sample ALY14, Alyki); (f) Granular texture in dunite (XPL, sample MG4, Megaplatanos). Abbreviations: Opx-Orthopyroxene, Cpx-Clinopyroxene, Ol-Olivine, Sp-Spinel, Mgt-Magnetite, XPL-Cross-polarized light, PPL-Plane-polarized light.

The most intensely serpentinised harzburgite and serpentinite display mainly mesh and lesser ribbon and bastitic textures; local interlocking, interpenetrating and hourglass textures occur as replacements on older serpentine. Besides serpentine, the secondary assemblage includes variable percentages of actinolite, magnetite and scarce talc, brucite, chlorite and calcite. Magnetite is regularly found in mesh cores, formed typically after olivine breakdown or in veins associated with serpentine. The less altered harzburgite contains relics of orthopyroxene porphyroclasts, olivine and Cr-spinel.

The cpx-rich harzburgite exhibits granular to porphyroclastic textures with olivine (50–70 vol. %), orthopyroxene (15–25 vol. %), clinopyroxene (4–5 vol. %) and spinel (up to 5%). In the samples with granular texture, olivine appears as anhedral grains, whereas in those with porphyroclastic texture, anhedral olivine may be partly corroded and replaced by olivine neoblasts. Clinopyroxene forms clusters and neoblastic grains in the recrystallized matrix.

The lherzolite displays mainly porphyroclastic texture and contains more than 5 vol. % clinopyroxene. Clinopyroxene may occur either as porphyroclasts with lobate boundaries and orthopyroxene exsolution lamellae (Figure 3d) or as isolated grains within the olivine matrix. Light-brown coloured spinel is of aluminous composition and forms disseminated anhedral crystals with lobate boundaries (Figure 3e).

The dunite is the least serpentinised rock among the studied ultramafics. They display granular texture with olivine (85–90 vol. %), orthopyroxene (up to 2%) and disseminated spinel (up to 10%). Coarse olivine grains (2.5–3.5 mm) are usually elongated and display undulatory extinction. Spinel grains are subhedral to euhedral, dark-red coloured and are heterogeneously distributed in the olivine matrix. Olivine may host spinel inclusions, whereas the opposite textural relationship was also observed. The least serpentinised dunite samples show protogranular texture with weakly deformed olivine crystals (Figure 3f) displaying undulose extinction or kink bands. The serpentinised dunite shows porphyroclastic to cataclastic textures with the predominance of fragmented olivine; fewer, disseminated Cr-spinel participate in its primary assemblage, too.

## 4.2. Mineral Chemistry

### 4.2.1. Spinel

Representative analyses of spinels from the investigated peridotites are given in Table 1. Cationic ratios were calculated on the basis of 32 oxygen atoms assuming spinel stoichiometry. The analysed spinels are unaltered and rather homogeneous in composition and do not show distinctive zoning from core to rim. Spinel grains in all types of investigated peridotites are classified as aluminous spinel, while the majority of spinel grains from Megaplatanos peridotites correspond to the composition of magnesiochromite (Figure 4a). However, to avoid any misunderstanding, in this study we use the term chromian spinel (Cr-spinel) for all these phases in different rock types.

The Cr-spinel from Megaplatanos dunite display high Cr# values ranging between 0.69 and 0.72 and their spots on a Cr# vs. Mg# [Mg/(Mg + Fe<sup>2+</sup>)] diagram form a separate cluster (Figure 4a). The Megaplatanos harzburgite hosts Cr-spinels with slightly lower Cr# values (varying between 0.35 and 0.52) relative to dunite but higher Cr# values relative to the other analysed harzburgitic spinels in this study. The Tragana harzburgite contains Cr-spinels of lower Cr# (0.35–0.45) and higher Mg# (0.59–0.73) similar to those of Ypato harzburgite with Cr# (0.36–0.43) and Mg# (0.60–0.68). The lherzolite and cpx-rich harzburgite of Alyki display Cr-spinels with the highest Mg# (0.69–0.73) similar to those of Tragana and the lowest Cr# (0.22–0.29) among the analysed Cr-spinels of this study, indicating a moderately fertile character (Figure 4a). Generally, it can be said that the Cr# values of Cr-spinel increase from lherzolite and cpx-rich harzburgite to harzburgite and dunite. On the other hand, the Mg# values increase from dunite and typical harzburgite to cpx-rich harzburgite and lherzolite. The TiO<sub>2</sub> content of the analysed Cr-spinels is low (0.1–0.2 wt. %), which is consistent with the relatively residual character of the studied peridotites.

The analysed Cr-spinels from the studied areas plot over a broad range of Cr# and Mg# showing linear covariation, similar to spinels from abyssal and Alpine-type peridotites and resemble those occurring in ultramafic rocks from Pindos, Vourinos, Othris, Koziakas, Iti and Kallidromon ophiolites (Figure 4b).

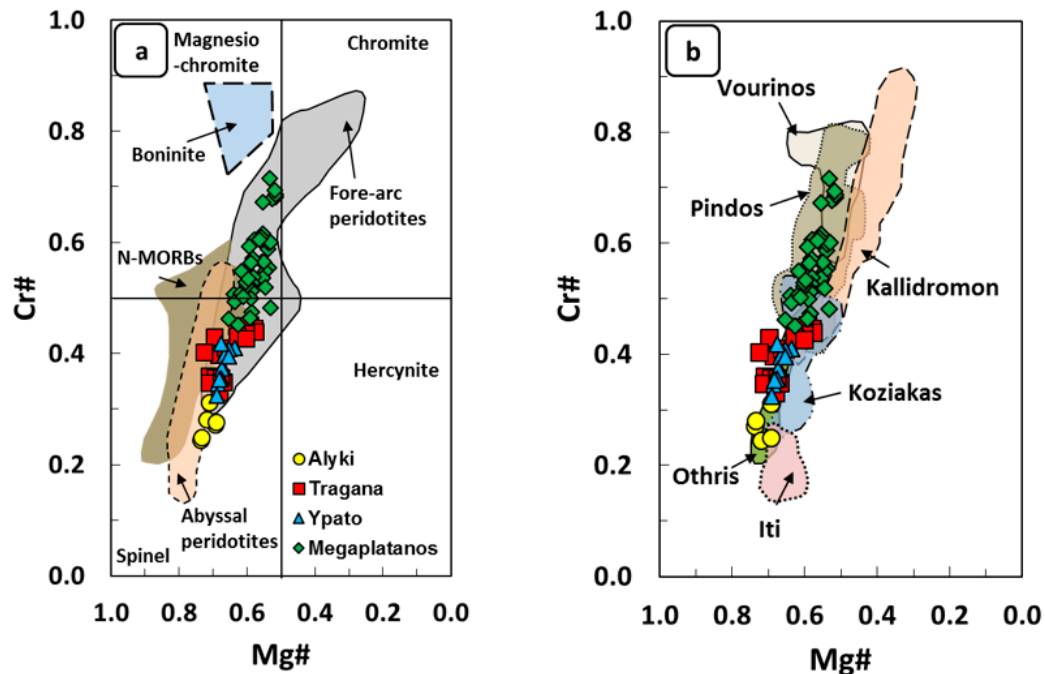


**Figure 4.** (a) Cr-spinel compositions from Lokris and Beotia peridotites, in terms of Cr# vs. Mg#. Data for spinel in modern abyssal peridotites are from [1,29]. Field for spinel in boninites is taken from [1]. Data for spinel in fore-arc peridotites are from [30,31]; (b) Comparison of Cr-spinel compositions from Lokris and Beotia peridotites with spinels from Othris, Pindos, Vourinos, Koziakas, Kallidromon and Iti ophiolites, on a Cr# against Mg# diagram (fields after [32–38]).

#### 4.2.2. Olivine

Representative analyses of olivine from the studied peridotites are given in Table 2. The analysed olivine are rather homogeneous in composition and do not show distinctive zoning from core to rim. Furthermore, no significant compositional difference between porphyroclasts and neoblasts has been observed. The forsterite content (Mg#) in the analysed crystals has a narrow compositional range between 91% and 92% in the harzburgite and dunite, which is close to that of olivine in abyssal peridotites (average Fo content: 91%; [1]) and is slightly lower in the lherzolite and cpx-rich harzburgite (90%–91%). In general, no major variations occur in the chemistry of olivine among the different lithologies of the investigated peridotites.

#### 4.2.3. Pyroxene

Representative analyses of pyroxenes from the studied peridotites are given in Table 2. The analysed pyroxenes consist of enstatitic orthopyroxene ( $\text{En}_{86.62-92.21}\text{Wo}_{0.53-5.45}$ ) and diopsidic clinopyroxene ( $\text{En}_{48.95-51.19}\text{Wo}_{46.03-47.44}$ ). They do not exhibit a systematic zoning and are rather chemically homogeneous. The Mg# values in orthopyroxene (0.92–0.96) and those in clinopyroxene (0.93–0.95) are similar, suggesting that Mg# is not strictly dependent on peridotite lithology. The enstatitic grains show slightly lower Cr# values (0.51–0.81) relative to the diopsidic ones (0.65–0.96). In general, Cr# values are more elevated in pyroxenes from the harzburgite compared to that from cpx-rich harzburgite and lherzolite.

**Table 1.** Representative electron microanalyses (wt.%) and atomic proportions of Cr-spinels from peridotites of Megaplatanos (MG), Tragana (TR), Ypato (YP) and Alyki (ALY).

Sample	MG2-4	MG3-24	MG4-12	MG4-23	MG5-14	MG5-23	TR5-9	TR5-14	TR6-1	TR6-8	TR14-3	TR14-7
Rock-Type	Harzb.	Harzb.	Dunite	Dunite	Harzb.	Harzb.	Harzb.	Harzb.	Harzb.	Harzb.	Harzb.	Harzb.
wt. %												
TiO <sub>2</sub>	0.20	-	0.18	0.16	-	0.15	0.15	-	0.12	0.18	0.10	-
Al <sub>2</sub> O <sub>3</sub>	26.52	23.10	14.64	15.53	27.71	28.22	37.96	33.78	30.07	30.77	33.37	33.54
FeO <sup>t</sup>	17.58	20.17	18.54	21.07	16.26	15.67	15.74	14.50	19.15	17.12	17.11	16.04
MgO	13.17	11.97	11.03	10.83	13.91	14.20	15.76	16.89	13.29	14.03	15.14	15.32
Cr <sub>2</sub> O <sub>3</sub>	42.92	44.75	54.92	52.48	42.63	40.94	30.33	34.03	37.01	37.51	34.70	34.68
Total	100.39	99.99	99.31	100.07	100.51	99.18	99.94	99.20	99.64	99.61	100.42	99.58
Formula units based on 32 oxygens												
Cr	1.021	1.091	1.404	1.329	1.004	0.971	0.682	0.776	0.872	0.878	0.794	0.797
Ti	0.005	0.000	0.004	0.004	0.000	0.003	0.003	0.000	0.003	0.004	0.002	0.000
Al	0.941	0.839	0.558	0.586	0.973	0.998	1.272	1.148	1.057	1.074	1.138	1.149
Fe <sup>3+</sup>	0.029	0.070	0.029	0.077	0.023	0.025	0.039	0.076	0.066	0.040	0.065	0.054
Fe <sup>2+</sup>	0.414	0.450	0.473	0.487	0.382	0.368	0.335	0.274	0.412	0.385	0.349	0.336
Mg	0.591	0.550	0.532	0.517	0.618	0.635	0.668	0.726	0.591	0.619	0.653	0.664
Total cat	3.000	3.000	3.000	3.000	3.000	3.000	3.000	3.000	3.000	3.000	3.000	3.000
Mg#	0.59	0.55	0.53	0.52	0.62	0.63	0.67	0.73	0.59	0.62	0.65	0.66
Cr#	0.52	0.57	0.72	0.69	0.51	0.49	0.35	0.40	0.45	0.45	0.41	0.41
Sample	YP2-1	YP2-12	YP2-14	YP2-16	YP2-19	YP2-21	ALY2-2	ALY2-6	ALY14-2	ALY14-12	ALY14-26	ALY27-10
Rock-Type	Harzb.	Harzb.	Harzb.	Harzb.	Harzb.	Harzb.	Lherz.	Lherz.	Lherz.	Lherz.	Lherz.	Dunite
wt. %												
TiO <sub>2</sub>	0.16	-	0.14	-	0.18	-	0.14	0.12	-	0.11	0.10	0.14
Al <sub>2</sub> O <sub>3</sub>	32.63	38.25	34.07	34.42	33.32	34.65	44.40	42.73	44.04	43.09	47.44	20.83
FeO <sup>t</sup>	17.43	14.91	16.13	15.81	15.49	16.31	13.93	15.50	14.65	14.94	13.99	20.28
MgO	13.77	16.10	15.18	15.42	15.69	15.21	16.86	16.62	17.19	16.78	18.03	12.04
Cr <sub>2</sub> O <sub>3</sub>	36.18	31.60	35.01	34.85	35.74	33.80	24.68	24.32	23.48	25.52	19.73	45.99
Total	100.17	100.86	100.53	100.50	100.42	99.97	100.01	99.29	99.36	100.44	99.29	99.28
Formula units based on 32 oxygens												
Cr	0.839	0.704	0.798	0.792	0.815	0.772	0.538	0.537	0.514	0.558	0.425	1.137
Ti	0.004	0.000	0.003	0.000	0.004	0.000	0.003	0.003	0.000	0.002	0.002	0.003
Al	1.128	1.269	1.158	1.166	1.133	1.179	1.444	1.406	1.437	1.403	1.523	0.768
Fe <sup>3+</sup>	0.026	0.027	0.038	0.041	0.044	0.049	0.012	0.051	0.049	0.034	0.049	0.088
Fe <sup>2+</sup>	0.401	0.324	0.351	0.339	0.329	0.345	0.309	0.311	0.290	0.311	0.270	0.442
Mg	0.602	0.676	0.652	0.661	0.675	0.655	0.693	0.692	0.710	0.691	0.732	0.561
Total cat	3.000	3.000	3.000	3.000	3.000	3.000	3.000	3.000	3.000	3.000	3.000	3.000
Mg#	0.60	0.68	0.65	0.66	0.67	0.65	0.69	0.69	0.71	0.69	0.73	0.56
Cr#	0.43	0.36	0.41	0.40	0.42	0.40	0.27	0.28	0.26	0.28	0.22	0.60

**Table 2.** Representative electron microprobe analyses (wt.%) and atomic proportions of olivine and pyroxene from peridotites of Megaplatanos (MG), Tragana (TR), Ypato (YP) and Alyki (ALY) study areas.

Sample	Olivine									Sample	Pyroxene								
	MG1-13	MG4-15	TR5-10	TR6-9	YP2-2	YP2-9	ALY2-7	ALY2-15	ALY27-20		MG1-10	MG5-6	TR5-12	TR14-9	YP2-3	YP2-5	ALY2-8	ALY14-11	
Rock-Type	Harzb.	Dunite	Harzb.	Harzb.	Harzb.	Harzb.	Lherz.	Lherz.	Dunite	Rock-Type	Harzb.	Harzb.	Harzb.	Harzb.	Harzb.	Harzb.	Lherz.	Lherz.	
wt. %										wt. %									
SiO <sub>2</sub>	39.90	39.03	41.25	41.34	40.84	40.34	40.92	39.95	41.15	SiO <sub>2</sub>	55.12	54.92	53.08	56.70	55.49	53.86	54.97	53.70	
TiO <sub>2</sub>	-	-	-	0.02	-	-	-	-	-	TiO <sub>2</sub>	-	-	0.20	-	-	-	-	-	0.31
Al <sub>2</sub> O <sub>3</sub>	-	-	-	-	-	-	0.18	-	0.02	Al <sub>2</sub> O <sub>3</sub>	1.78	0.86	2.86	3.83	2.57	2.30	3.57	3.50	
FeO	8.35	8.43	8.02	8.85	8.74	8.56	8.98	9.14	8.19	FeO	6.68	1.82	2.03	5.18	5.85	1.82	5.41	2.26	
MgO	50.99	51.62	50.40	50.36	51.10	51.02	50.04	50.47	50.99	MgO	35.41	18.81	17.12	34.39	34.84	18.11	33.15	17.18	
CaO	-	-	-	-	-	-	0.10	-	-	CaO	0.29	23.53	22.82	-	0.69	23.09	2.90	23.17	
Cr <sub>2</sub> O <sub>3</sub>	0.27	0.22	-	-	-	-	0.13	-	0.22	Cr <sub>2</sub> O <sub>3</sub>	0.81	0.82	0.96	-	0.51	0.65	0.69	0.80	
NiO	-	-	-	-	0.22	0.38	-	-	-	Total	100.09	100.76	99.07	100.10	99.95	99.83	100.69	100.92	
Total	99.51	99.30	99.67	100.57	100.90	100.30	100.35	99.56	100.57										
Formula units based on 4 oxygens										Formula units based on 6 oxygens									
Si	0.978	0.962	1.004	1.001	0.988	0.983	1.244	0.982	0.995	Si	1.892	1.972	1.938	1.935	1.905	1.949	1.883	1.926	
Al	-	-	-	-	-	-	0.006	-	0.001	Ti	-	-	0.005	-	-	-	-	0.008	
Ti	-	-	-	-	-	-	-	-	-	Al	0.072	0.036	0.123	0.154	0.104	0.098	0.144	0.148	
Fe <sup>2+</sup>	0.171	0.174	0.163	0.179	0.177	0.174	0.228	0.188	0.166	Fe <sup>3+</sup>	0.122	-	-	-	0.071	-	0.071	-	
Mg	1.864	1.896	1.829	1.818	1.843	1.853	2.267	1.849	1.838	Fe <sup>2+</sup>	0.069	0.055	0.062	0.148	0.097	0.055	0.084	0.068	
Ca	-	-	-	-	-	-	0.003	-	-	Cr	0.022	0.023	0.028	-	0.014	0.019	0.019	0.023	
Ni	-	-	-	-	0.004	0.007	-	-	-	Mg	1.812	1.007	0.932	1.750	1.783	0.977	1.693	0.918	
Cr	0.005	0.004	-	-	-	-	0.003	-	0.004	Ca	0.011	0.905	0.893	-	0.025	0.895	0.106	0.890	
Mg#	0.92	0.92	0.92	0.91	0.91	0.91	0.91	0.91	0.92	Wo	0.53	46.03	47.32	-	1.28	46.45	5.45	47.44	
										En	89.95	51.19	49.39	92.21	90.22	50.69	86.62	48.95	
										Fs	9.52	2.78	3.29	7.79	8.50	2.86	7.93	3.61	
										Mg#	0.96	0.95	0.94	0.92	0.95	0.95	0.95	0.93	

## 5. Discussion

### 5.1. Partial Melting and Geotectonic Setting

Lokris and Beotia ophiolite bodies are part of the Hellenic ophiolites. The Dinaric–Hellenic ophiolites have been mostly originated in SSZ settings during the early–late Jurassic period, e.g., [9,39–47]. Mineral chemistry from the investigated peridotites of Lokris and Beotia ophiolite occurrences reveals a multi-stage genesis in the different types of their host peridotites. The last are characterized by variable clinopyroxene contents, a fact that provides direct evidence of the extent of their depletion [48]. Peridotites from Megaplatanos, Tragana, and Ypato have low clinopyroxene abundances (<4 vol. %) resembling mantle peridotites, which are formed by high degrees of melting. This signature is in agreement with the high olivine modal abundances (65–80 vol. %), the low  $\text{Al}_2\text{O}_3$  contents in pyroxenes and the forsterite-rich nature of olivine (Fo: 91%–92%). On the other hand, peridotites from Alyki that have higher clinopyroxene content (4–10 vol. %) imply an origin from small to moderate degrees of melt extraction (5%–15% partial melting), e.g., [49,50].

The considerable differences among the investigated peridotites can best be illustrated with the plot of Cr# in spinel versus Fo content in olivine (OSMA: Olivine Spinel Mantle Array; [5]; Figure 5a). The olivine compositions correlate with the spinel ones within OSMA, confirming the mantle residue origin of the investigated peridotites. Specifically, the spinel Cr# increases as olivine Fo increases, such that the spinel–olivine pairs from the investigated harzburgite, dunite, cpx-rich harzburgite and lherzolite lie within the olivine–spinel mantle array of [5].

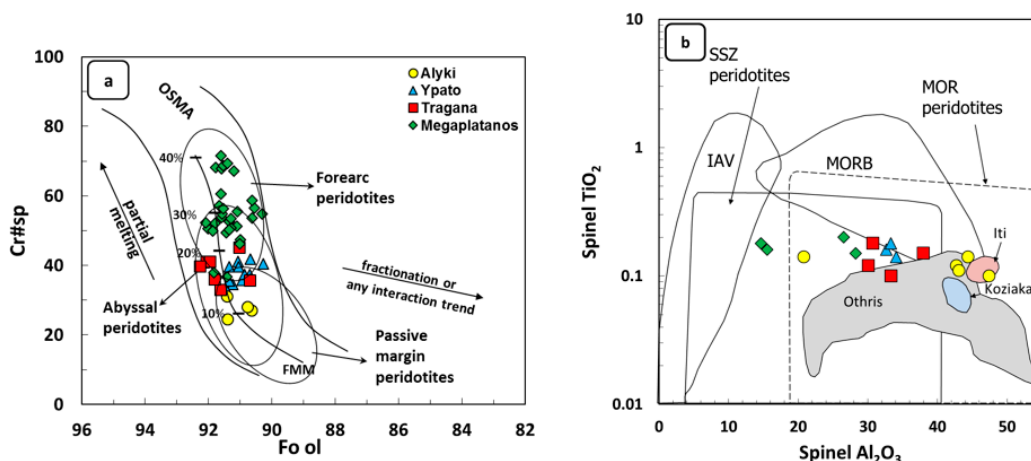


**Figure 5.** (a) Compositional relationship between Fo content of olivine and Cr#s of coexisting Cr-spinels of mantle peridotitic rocks from Lokris and Beotia; the olivine–spinel mantle array (OSMA) is after [2]; (b) Binary diagram of  $\text{TiO}_2$  (wt. %) vs.  $\text{Al}_2\text{O}_3$  (wt. %) contents for spinels from Lokris and Beotia peridotites. Fields for mid-ocean ridge basalts (MORB) and island arc volcanics (IAV), as well as MOR and supra-subduction zone (SSZ) peridotites according to [7]. Field for spinels from Iti, Othris and Koziakas peridotites are according to [35–39]. Legend as in Figure 5a.

The Cr-spinel, which serves as another useful phase for the estimation of partial melting processes in mantle peridotites [5,51], show distinct compositions between the different types of peridotites of Lokris and Beotia ophiolite occurrences. The Cr-spinel hosted in the lherzolite and cpx-rich harzburgite of Alyki is represented by higher Mg# and lower Cr#, suggesting 9%–14% partial melting. On the other hand, the harzburgite of Megaplatanos contain Cr-spinel with lower Mg# and higher Cr#, suggesting 22%–35% partial melting, while the Cr-spinel from the dunite of Megaplatanos contains the lowest Mg# and highest Cr# values between the analysed samples and form a separate cluster suggesting 36%–40% partial melting (Figure 5a). The Cr-spinel from the harzburgite of Tragana and Ypato contain intermediate values of Cr# and Mg# between those of peridotites from Megaplatanos and Alyki,

suggesting 15%–22% partial melting (Figure 5a). The same diagram shows that the analysed samples plot within two different fields (Figure 5a). The Cr-spinels from the harzburgite and dunite from Megaplatanos plot mainly within the field for fore-arc peridotites, whereas those from the harzburgite from Ypato and Tragana, as well as from the lherzolite and cpx-rich harzburgite from Alyki fall within the field of abyssal and passive margin peridotites.

The generally low Ti contents also support the relatively residual character of the investigated peridotites. Titanium is incompatible during partial melting and its content is expected to decrease as the melting degree increases [52–55]. On the basis of TiO<sub>2</sub> and Al<sub>2</sub>O<sub>3</sub> contents of their unaffected cores, the studied Cr-spinels hosted in harzburgite and dunite resemble those occurring in back-arc settings, since they plot within common fields of SSZ and MORB peridotites (Figure 5b). However, Cr-spinels from Alyki indicate a MORB environment and resemble those occurring in lherzolites from Iti, Othris and Koziakas ophiolites (Figure 5b) [35–39].

The modal and elemental composition of the mineral constituents of mantle peridotites are dependent on the geotectonic environment of their formation. Cr# in spinel is also a good indicator of the tectonomagmatic history of the host rock. Cr-spinel grains hosted in the lherzolite, cpx-rich harzburgite and harzburgite of Alyki, Tragana, Ypato and Megaplatanos display low Cr#, similar to those from oceanic peridotites (including back-arc basins; [1]), while Cr-spinel compositions from harzburgite and particularly dunite of Megaplatanos (Cr#>0.6) are consistent with a SSZ origin. It has been shown that fore-arc regions may contain both SSZ and abyssal peridotites, although the former are typically dominant [48,55–57]. Mantle peridotites from SSZ environments are characterized by depleted harzburgite, comprising spinels mostly with Cr#>0.50 and low TiO<sub>2</sub> contents [46,56–59]. Thus, the Megaplatanos-investigated peridotites may represent the residues of higher degrees of melting of previously depleted harzburgites from the mantle wedge above a subduction zone. On the other hand, the harzburgite, cpx-rich harzburgite and lherzolite from Tragana, Ypato and Alyki represent less depleted mantle peridotites, formed by lower degrees of melting. This does not imply that the mantle sections of Lokris and Beotia ophiolites started with identical compositions and that their differences are derived entirely from the most recent episodes of partial melting. The mantle section of many ophiolites contains clearly compositionally heterogeneous peridotites, e.g., [60–62], which display mineralogical, textural and compositional evidence for complex, multi-phase melting, depletion and enrichment processes in their petrogenetic history [63,64].

Moreover, the studied Cr-spinels hosted in the harzburgite and dunite resemble those occurring in ultramafic rocks from Pindos and Othris ophiolites, while the Cr-spinels from Alyki resemble those occurring in lherzolites from Iti, Kallidromon, Othris and Koziakas ophiolites that have been interpreted as being formed (entirely or partially) in SSZ settings [32–39,44,65], thus pointing to a similar origin.

## 5.2. Geothermobarometry

Equilibration temperatures for the studied peridotites have been calculated using core compositions from all the mantle phases (Supplementary Table). Regarding orthopyroxene grains, care was taken to analyse porphyroclasts free of clinopyroxene exsolution lamellae. Application of the two-pyroxene geothermometer of [66] yielded temperatures varying between 881 and 999 °C assuming a pressure of 0.7 GPa, which is usual for upper mantle peridotites. Using the partitioning of Mg and Fe<sup>2+</sup> between olivine and spinel of [67], the calculated temperature values are significantly lower and range between 761 and 787 °C for dunite, 740 and 778 °C for harzburgite and 697 and 715 °C for cpx-rich harzburgite and lherzolite. All the above estimated temperatures are closing temperatures as there is a lack of compositional equilibrium among the phases in the peridotite assemblages. The observed scatter and the lower values given by the olivine–spinel geothermometer may be due to recrystallization and/or different rates of diffusion between the mineral pairs used in thermometry.

The two-pyroxene geobarometer suggested by [68] was used to determine the pressure conditions under which the Lokris and Beotia peridotites could have formed. The estimated pressure values range between 0.7 and 0.8 GPa for Megaplatanos and 0.5–0.6 GPa for the Alyki, Tragana and Ypato peridotites. Pressure values close to 0.8 GPa are consistent with the spinel stability field in the mantle, which lies in a pressure range between 0.8 and 2 GPa [69]. However, the lower values could imply a low-pressure refertilization process of the depleted harzburgite that following recrystallization, led to the formation of cpx-rich harzburgite and lherzolite [70].

## 6. Conclusions

Accessory Cr-spinels grains from ultramafic rocks from Lokris (Megaplatanos and Tragana), and Beotia (Ypato and Alyki) ophiolitic occurrences were studied. The ultramafic bodies comprise principally harzburgite with minor dunite. Harzburgite is commonly moderately serpentinised, whereas locally it is unaltered. Small amounts of cpx-rich harzburgite grading to lherzolite have been observed along with the harzburgite in Alyki. The investigated peridotites show mainly porphyroclastic and granular textures followed by plastic deformation features, similar to those of Alpine-type upper mantle peridotites.

Cr-spinel grains hosted in harzburgite and cpx-rich harzburgite to lherzolite display low Cr#, typical for oceanic (including back-arc basins) ophiolites, whereas Cr-spinels of harzburgite and dunite from Megaplatanos with relatively higher Cr# characterize arc-related ophiolitic sequences. The studied Cr-spinels from the Alyki indicate a moderately fertile character, analogous to those from abyssal peridotites. Cr-rich spinels from Megaplatanos are restricted at higher Cr# values, possessing slightly lower Mg# values. All the studied Cr-spinels are similar to those from Alpine-type peridotites.

Cr-spinel–olivine pairs from the investigated peridotites plot within the OSMA (olivine–spinel mantle array). Linear variation of the spinel Cr# and forsterite content of olivine is consistent with a SSZ origin, indicating a residual origin of the peridotites. Harzburgite and dunite from Megaplatanos may represent the residues of higher degrees of partial melting of previously depleted harzburgite from the mantle wedge above a subduction zone. Textural evidence is in agreement with a melt–peridotite interaction after a partial melting event. On the other hand, harzburgite, cpx-rich harzburgite and lherzolite from Tragana, Ypato and Alyki represent less depleted mantle peridotites, formed by lower degrees of partial melting, implying mantle heterogeneity in the Lokris and Beotia ophiolite slices.

Equilibration temperatures for the studied peridotites have been calculated using the two-pyroxene geothermometer and the partitioning of Mg and Fe<sup>2+</sup> between olivine and spinel yielded temperatures varying between 875 and 999 °C and 679 and 787 °C respectively, assuming a pressure of 0.7 GPa. The application of a two-pyroxene geobarometer gave pressure values between 0.5 and 0.8 GPa.

**Supplementary Materials:** The following are available online at [www.mdpi.com/2076-3263/7/1/10/s1](http://www.mdpi.com/2076-3263/7/1/10/s1).

**Acknowledgments:** This research has been supported by SARG (Special Account for Research Grants) of the National and Kapodistrian University of Athens. Two anonymous reviewers are kindly thanked for their constructive criticism that led to the improvement of the current manuscript. We would also like to thank Academic Editor Basilios Tsikouras, for his thorough editorial review that helped to enhance the quality of the manuscript.

**Author Contributions:** Panagiotis Pomonis and Andreas Magganas performed the fieldwork. Panagiotis Pomonis processed and analysed the data. Panagiotis Pomonis and Andreas Magganas wrote the paper.

**Conflicts of Interest:** The authors declare no conflict of interest.

## References

1. Dick, H.J.B.; Bullen, T. Chromium spinel as a petrogenetic indicator in abyssal and alpine-type peridotites and spatially associated lavas. *Contrib. Mineral. Petr.* **1984**, *86*, 54–76. [[CrossRef](#)]
2. Arai, S. Chemistry of chromium spinel in volcanic rocks as a potential guide to magma chemistry. *Mineral. Mag.* **1992**, *56*, 173–184. [[CrossRef](#)]

3. Arai, S. Compositional variation of olivine-chromian spinel in Mg-rich magmas as a guide to their residual spinel peridotites. *J. Volcanol. Geoth. Res.* **1994**, *59*, 279–293. [[CrossRef](#)]
4. Arai, S.; Okamura, H.; Kadoshima, K.; Tanaka, C.; Suzuki, K.; Ishimaru, S. Chemical characteristics of chromian spinel in plutonic rocks: Implications for deep magma processes and discrimination of tectonic setting. *Island Arc* **2011**, *20*, 125–137. [[CrossRef](#)]
5. Arai, S. Characterization of spinel peridotites by olivine-spinel compositional relationships: Review and interpretation. *Chem. Geol.* **1994**, *113*, 191–204. [[CrossRef](#)]
6. Barnes, S.J.; Roeder, P.L. The range of spinel compositions in terrestrial mafic and ultramafic rocks. *J. Petrol.* **2001**, *42*, 2279–2302. [[CrossRef](#)]
7. Kamenetsky, V.S.; Crawford, A.J.; Meffre, S. Factors controlling chemistry of magmatic spinel: An empirical study of associated olivine, Cr-spinel and melt inclusions from primitive rocks. *J. Petrol.* **2001**, *42*, 655–671. [[CrossRef](#)]
8. Pal, T. Petrology and geochemistry of the Andaman ophiolite: Melt–rock interaction in a suprasubduction-zone setting. *J. Geol. Soc. London* **2011**, *168*, 1031–1045. [[CrossRef](#)]
9. Picazo, S.; Müntener, O.; Manatschal, G.; Bauville, A.; Karner, G.; Johnson, C. Mapping the nature of mantle domains in Western and Central Europe based on clinopyroxene and spinel chemistry: Evidence for mantle modification during an extensional cycle. *Lithos* **2016**, *266*, 233–263. [[CrossRef](#)]
10. Rollinson, H. The geochemistry of mantle chromitites from the northern part of the Oman ophiolite: inferred parental melt compositions. *Contrib. Mineral. Petr.* **2008**, *156*, 273–288. [[CrossRef](#)]
11. Uysal, İ.; Ersoy, E.Y.; Karşlı, O.; Dilek, Y.; Sadıklar, M.B.; Ottley, C.J.; Tiepolo, M.; Meisel, T. Coexistence of abyssal and ultra-depleted SSZ type mantle peridotites in a Neo-Tethyan Ophiolite in SW Turkey: Constraints from mineral composition, whole-rock geochemistry (major–trace–REE–PGE), and Re–Os isotope systematics. *Lithos* **2012**, *132*, 50–69. [[CrossRef](#)]
12. Zhou, M.; Robinson, P.T. Origin and tectonic environment of podiform chromite deposits. *Econ. Geol.* **1997**, *92*, 259–262. [[CrossRef](#)]
13. Arai, S. Origin of podiform chromitites. *J. Asian Earth Sci.* **1997**, *15.2*, 303–310. [[CrossRef](#)]
14. Ballhaus, C. Origin of podiform chromite deposits by magma mingling. *Earth. Planet. Sc. Lett.* **1998**, *156.3*, 185–193. [[CrossRef](#)]
15. González-Jiménez, J.M.; Proenza, J.A.; Gervilla, F.; Melgarejo, J.C.; Blanco-Moreno, J.A.; Ruiz-Sánchez, R.; Griffin, W.L. High-Cr and high-Al chromitites from the Sagua de Tánamo district, Mayarí-Cristal ophiolitic massif (eastern Cuba): Constraints on their origin from mineralogy and geochemistry of chromian spinel and platinum-group elements. *Lithos* **2011**, *125*, 101–121. [[CrossRef](#)]
16. Melcher, F.; Grum, W.; Simon, G.; Thalhammer, T.V.; Stumpfl, E.F. Petrogenesis of the ophiolitic giant chromite deposits of Kempirsai, Kazakhstan: A study of solid and fluid inclusions in chromite. *J. Petrol.* **1997**, *38*, 1419–1458. [[CrossRef](#)]
17. Melcher, F.; Grum, W.; Thalhammer, T.V.; Thalhammer, O.A.R. The giant chromite deposits at Kempirsai, Urals: Constraints from trace element (PGE, REE) and isotope data. *Miner. Deposita* **1999**, *34*, 250–272. [[CrossRef](#)]
18. Proenza, J.A.; Ortega-Gutiérrez, F.; Camprubí, A.; Tritlla, J.; Elias-Herrera, M.; Reyes-Salas, M. Paleozoic serpentinite-enclosed chromitites from Tehuiztingo (Acatlán Complex, southern Mexico): A petrological and mineralogical study. *J. S. Am. Earth Sci.* **2004**, *16*, 649–666. [[CrossRef](#)]
19. Uysal, İ.; Kaliwoda, M.; Karşlı, O.; Tarkian, M.; Sadıklar, M.B.; Ottley, C.J. Compositional variations as a result of partial melting and melt–peridotite interaction in an upper mantle section from the Ortaca area, southwestern Turkey. *Can. Mineral.* **2007**, *45*, 1471–1493. [[CrossRef](#)]
20. Uysal, İ.; Sadıklar, M.B.; Tarkian, M.; Karşlı, O.; Aydın, F. Mineralogy and composition of the chromitites and their platinum-group minerals from Ortaca (Muğla-SW Turkey): Evidence for ophiolitic chromitite genesis. *Miner. Petrol.* **2005**, *83*, 219–242. [[CrossRef](#)]
21. Zaccarini, F.; Garuti, G.; Proenza, J.A.; Campos, L.; Thalhammer, O.A.; Aiglsperger, T.; Lewis, J.F. Chromite and platinum group elements mineralization in the Santa Elena Ultramafic Nappe (Costa Rica): geodynamic implications. *Geol. Acta* **2011**, *9*.
22. Zhou, M.; Robinson, P.T.; Bai, W.J. Formation of podiform chromitites by melt/rock interaction in the upper mantle. *Miner. Deposita* **1994**, *29*, 98–101.

23. Zhou, M.F.; Sun, M.; Keays, R.R.; Kerrich, R.W. Controls on platinum-group elemental distributions of podiform chromitites: A case study of high-Cr and high-Al chromitites from Chinese orogenic belts. *Geochim. Cosmochim. Ac.* **1998**, *62*, 677–688. [[CrossRef](#)]
24. Voigt, M.; Von Der Handt, A. Influence of subsolidus processes on the chromium number in spinel in ultramafic rocks. *Contrib. Mineral. Petr.* **2011**, *162*, 675–689. [[CrossRef](#)]
25. Robertson, A.H.F.; Clift, P.D.; Degnan, P.J.; Jones, G. Palaeogeographic and palaeotectonic evolution of the Eastern Mediterranean Neotethys. *Palaeogeogr. Palaeoclimatol. Palaeoeco.* **1991**, *87*, 289–343. [[CrossRef](#)]
26. Smith, A.G. Othris, Pindos and Vourinos ophiolites and the Pelagonian zone. In Proceedings of the 6th Colloquium on the Geology of the Aegean Region, Athens, Greece, 27 September 1977; pp. 1369–1374.
27. Robertson, A.H. Overview of the genesis and emplacement of Mesozoic ophiolites in the Eastern Mediterranean Tethyan region. *Lithos* **2002**, *65*, 1–67. [[CrossRef](#)]
28. Stampfli, G.M.; Hochard, C. Plate tectonics of the Alpine realm. *Geol. Soc. Lond. Spec. Publ.* **2009**, *327*, 89–111. [[CrossRef](#)]
29. Juteau, T.; Berger, E.; Cannat, M. Serpentinized, Residual Mantle Peridotites from the M.A.R. Median Valley, ODP Hole 670A (21° 10'N, 45° 02'W): Primary Mineralogy and Geothermometry. Available online: [http://www-odp.tamu.edu/Publications/106109SR/VOLUME/CHAPTERS/sr106109\\_04.pdf](http://www-odp.tamu.edu/Publications/106109SR/VOLUME/CHAPTERS/sr106109_04.pdf) (accessed on 3 March 2017).
30. Ishii, T.; Robinson, P.T.; Maekawa, H.; Fiske, R. Petrological Studies of Peridotites From Diapiric Serpentinite Seamounts in the Izu–Mariana fore-arc, Leg 125. Available online: [http://www-odp.tamu.edu/publications/125\\_SR/VOLUME/CHAPTERS/sr125\\_27.pdf](http://www-odp.tamu.edu/publications/125_SR/VOLUME/CHAPTERS/sr125_27.pdf) (accessed on 3 March 2017).
31. Ohara, Y.; Ishii, T. Peridotites from the southern Mariana forearc: heterogeneous fluid supply in the mantle wedge. *Isl. Arc* **1998**, *7*, 541–558. [[CrossRef](#)]
32. Economou-Eliopoulos, M.; Vacondios, I. Geochemistry of chromitites and host rocks from the Pindos ophiolite complex, northwestern Greece. *Chem. Geol.* **1995**, *122*, 99–108. [[CrossRef](#)]
33. Economou-Eliopoulos, M.; Tarkian, M.; Sambanis, G. On the geochemistry of chromitites from the Pindos ophiolite complex, Greece. *Chem. Erde* **1999**, *59*, 19–31.
34. Kapsiotis, A.N. Mineralogy, geochemistry and geotectonic significance of harzburgites from the southern Dramala upper mantle suite, Pindos ophiolite complex, NW Greece. *Geol. J.* **2014**, *51*, 236–262. [[CrossRef](#)]
35. Karipi, S.; Tsikouras, B.; Hatzipanagiotou, K.; Grammatikopoulos, T. Petrogenetic significance of spinel-group minerals from the ultramafic rocks of the Iti and Kallidromon ophiolites (Central Greece). *Lithos* **2007**, *99*, 136–149. [[CrossRef](#)]
36. Magganas, A.; Koutsovitis, P. Composition, melting and evolution of the upper mantle beneath the Jurassic Pindos ocean inferred by ophiolitic ultramafic rocks in East Othris, Greece. *Int. J. Earth Sci.* **2015**, *104*, 1185–1207. [[CrossRef](#)]
37. Pomonis, P.; Tsikouras, B.; Hatzipanagiotou, K. Petrogenetic evolution of the Koziakas ophiolite complex (W. Thessaly, Greece). *Miner. Petrol.* **2007**, *89*, 77–111. [[CrossRef](#)]
38. Hatzipanagiotou, K.; Pomonis, P.; Tsikouras, B. Origin and evolution of ultramafic rocks from the Koziakas ophiolite, continental Greece. *Braunschweiger geowiss Arb* **2001**, *24*, 235–247.
39. Barth, M.G.; Mason, P.R.; Davies, G.R.; Dijkstra, A.H.; Drury, M.R. Geochemistry of the Othris ophiolite, Greece: Evidence for refertilization? *J. Petrol.* **2003**, *44*, 1759–1785. [[CrossRef](#)]
40. Bortolotti, V.; Chiari, M.; Marcucci, M.; Marroni, M.; Pandolfi, L.; Principi, G.; Saccani, E. Comparison among the Albanian and Greek ophiolites: In search of constraints for the evolution of the Mesozoic Tethys Ocean. *Ophioliti* **2004**, *29*, 19–35.
41. Koutsovitis, P.; Magganas, A.; Pomonis, P.; Ntaflos, T. Subduction-related rodingites from East Othris, Greece: Mineral reactions and physicochemical conditions of formation. *Lithos* **2013**, *172–173*, 139–157. [[CrossRef](#)]
42. Karipi, S.; Tsikouras, B.; Hatzipanagiotou, K. The petrogenesis and tectonic setting of ultramafic rocks from Iti and Kallidromon Mountains, continental Central Greece: Vestiges of the Pindos Ocean. *Can. Mineral.* **2006**, *44*, 267–287. [[CrossRef](#)]
43. Tsikouras, B.; Karipi, S.; Rigopoulos, I.; Perraki, M.; Pomonis, P.; Hatzipanagiotou, K. Geochemical processes and petrogenetic evolution of rodingite dykes in the ophiolite complex of Othrys (Central Greece). *Lithos* **2009**, *113*, 540–554. [[CrossRef](#)]

44. Rassios, A.H.; Moores, E.M. Heterogeneous mantle complex, crustal processes, and obduction kinematics in a unified Pindos-Vourinos ophiolitic slab (northern Greece). *Geol. Soc. Lond. Spec. Publ.* **2006**, *260*, 237–266. [[CrossRef](#)]
45. Rassios, A.; Smith, A.G. Constraints on the formation and emplacement age of western Greek ophiolites (Vourinos, Pindos, and Othris) inferred from deformation structures in peridotites. *Geol. S. Am. S.* **2000**, 473–484.
46. Smith, A.G. Tectonic significance of the Hellenic-Dinaric ophiolites. *Geol. Soc. Lond. Spec. Publ.* **1993**, *76*, 213–243. [[CrossRef](#)]
47. Smith, A.G. Tethyan ophiolite emplacement, Africa to Europe motions, and Atlantic spreading. *Geol. Soc. Lond. Spec. Publ.* **2006**, *260*, 11–34. [[CrossRef](#)]
48. Parkinson, I.J.; Pearce, J.A. Peridotites of the Izu-Bonin-Mariana forearc (ODP Leg 125) evidence for mantle melting and melt–mantle interactions in a suprasubduction zone setting. *J. Petrol.* **1998**, *39*, 1577–1618. [[CrossRef](#)]
49. Dokuz, A.; Uysal, I.; Kaliwoda, M.; Karsli, O.; Ottley, C.J.; Kandemir, R. Early abyssal- and late SSZ-type vestiges of the Rheic oceanic mantle in the Variscanbasement of the Sakarya Zone, NE Turkey: Implications for the sense of subduction and opening of the Paleotethys. *Lithos* **2011**, *127*, 176–191. [[CrossRef](#)]
50. Seyler, M.; Lorand, J.P.; Dick, H.J.B.; Drouin, M. Pervasive melt percolation reactions in ultra-depleted refractory harzburgites at the Mid-Atlantic Ridge, 15°20N: ODP Hole 1274A. *Contrib. Miner. Petrol.* **2007**, *153*, 303–319. [[CrossRef](#)]
51. Bédard, J.H.; Leclerc, F.; Harris, L.B.; Goulet, N. Intra-sill magmatic evolution in the Cummings Complex, Abitibi greenstone belt: Tholeiitic to calc-alkaline magmatism recorded in an Archaean subvolcanic conduit system. *Lithos* **2009**, *111*, 47–71. [[CrossRef](#)]
52. Choi, S.H.; Shervais, J.W.; Mukasa, S.B. Supra-subduction and abyssal mantle peridotites of the Coast Range ophiolite, California. *Contrib. Mineral. Petrol.* **2008**, *156*, 551–576. [[CrossRef](#)]
53. Kinzler, R.J.; Grove, T.L. Primary magmas of mid-ocean ridge basalts 1. Experiments and methods. *J. Geophys. Res. Solid Earth* **1992**, *97*, 6885–6906. [[CrossRef](#)]
54. Langmuir, C.H.; Klein, E.M.; Plank, T. Petrological systematics of mid-ocean ridge basalts: Constraints on melt generation beneath ocean ridges. In *Mantle Flow and Melt Generation at Mid-Ocean Ridges*; John Wiley & Sons, Inc.: Hoboken, NJ, USA, 1993; pp. 183–280.
55. Pearce, J.A.; Barker, P.F.; Edwards, S.J.; Parkinson, I.J.; Leat, P.T. Geochemistry and tectonic significance of peridotites from the South Sandwich arc-basin system, south Atlantic. *Contrib. Mineral. Petr.* **2000**, *139*, 36–53. [[CrossRef](#)]
56. Ghosh, B.; Morishita, T.; Bhatta, K. Significance of chromian spinels from the mantle sequence of the Andaman Ophiolite, India: Paleogeodynamic implications. *Lithos* **2013**, *164*, 86–96. [[CrossRef](#)]
57. Parkinson, I.J.; Pearce, J.A.; Thirwall, M.F.; Johnson, K.T.M.; Ingram, G. Trace Element Geochemistry of Peridotites from the Izu-Bonin-Mariana forearc, Leg 125. Available online: [http://www-odp.tamu.edu/publications/125\\_SR/VOLUME/CHAPTERS/sr125\\_28.pdf](http://www-odp.tamu.edu/publications/125_SR/VOLUME/CHAPTERS/sr125_28.pdf) (accessed on 3 March 2017).
58. Bloomer, S.H.; Hawkins, J.W. Gabbroic and ultramafic rocks from the Mariana Trench: An island arc ophiolite. In *The Tectonic and Geologic Evolution of Southeast Asian Seas and Islands: Part 2*; John Wiley & Sons, Inc.: Hoboken, NJ, USA, 1983; pp. 294–317.
59. Bizimis, M.; Salters, V.J.M.; Bonatti, E. Trace and REE content of clinopyroxenes from supra-subduction zone peridotites. Implications for melting and enrichment processes in island arcs. *Chem. Geol.* **2000**, *165*, 67–85. [[CrossRef](#)]
60. Stern, R.J. The anatomy and ontogeny of modern intra-oceanic arc systems. *Geol. Soc. Lond. Spec. Publ.* **2010**, *338*, 7–34. [[CrossRef](#)]
61. Pearce, J.A.; Lippard, S.J.; Roberts, S. Characteristics and tectonic significance of supra-subduction zone ophiolites. *Geol. Soc. Lond. Spec. Publ.* **1984**, *16*, 77–94. [[CrossRef](#)]
62. Khedr, M.Z.; Arai, S.; Python, M.; Tamura, A. Chemical variations of abyssal peridotites in the central Oman ophiolite: Evidence of oceanic mantle heterogeneity. *Gondwana Res.* **2014**, *25*, 1242–1262. [[CrossRef](#)]
63. Yang, J.S.; Robinson, P.T.; Dilek, Y. Diamonds in ophiolites. *Elements* **2014**, *10*, 127–130. [[CrossRef](#)]
64. Uysal, I.; Ersoy, E.Y.; Dilek, Y.; Kapsiotis, A.; Sarifakioğlu, E. Multiple episodes of partial melting, depletion, metasomatism and enrichment processes recorded in the heterogeneous upper mantle sequence of the Neotethyan Eldivan ophiolite, Turkey. *Lithos* **2016**, *246*, 228–245. [[CrossRef](#)]

65. Moghadam, H.S.; Khedr, M.Z.; Arai, S.; Sternd, R.J.; Ghorbani, G.; Tamura, A.; Ottley, C.J. Arc-related harzburgite–dunite–chromitite complexes in the mantle section of the Sabzevar ophiolite, Iran: A model for formation of podiform chromitites. *Gondwana Res.* **2013**, *27*, 575–593. [[CrossRef](#)]
66. Brey, G.P.; Köhler, T. Geothermobarometry in four-phase lherzolites. II. New thermobarometers and practical assessment of existing thermobarometers. *J. Petrol.* **1990**, *31*, 1353–1378. [[CrossRef](#)]
67. Fabries, I. Spinel-olivine geothermometry in peridotites from ultramafic complexes. *Contrib. Mineral. Petr.* **1979**, *69*, 329–336. [[CrossRef](#)]
68. Putirka, K.D. Thermometers and Barometers for volcanic systems. *Rev. Miner. Geochem.* **2008**, *69*, 61–120. [[CrossRef](#)]
69. Gasparik, T. Orthopyroxene thermometry in simple and complex systems. *Contrib. Mineral. Petr.* **1987**, *96*, 357–370. [[CrossRef](#)]
70. Elthon, D. Chemical trends in abyssal peridotites: Refertilization of depleted suboceanic mantle. *J. Geophys. Res.* **1992**, *97*, 9015–9025. [[CrossRef](#)]



© 2017 by the authors. Licensee MDPI, Basel, Switzerland. This article is an open access article distributed under the terms and conditions of the Creative Commons Attribution (CC BY) license (<http://creativecommons.org/licenses/by/4.0/>).